Journal of Engineering Mathematics (2006) 54: 31–48
DOI 10.1007/s10665-005-3536-4

Hydroelastic behavior of a floating ring-shaped plate

ALEXEY I. ANDRIANOV and AAD J. HERMANS
Department of Applied Mathematics, Faculty of Electrical Engineering, Mathematics and Computer Science, Delft University of Technology, Mekelweg 4, 2628 CD Delft, The Netherlands
(a.i.andrianov@ewi.tudelft.nl; a.j.hermans@ewi.tudelft.nl)

Received 26 July 2004; accepted in revised form 10 March 2005

Abstract. The interaction between incident surface water waves and floating elastic plate is studied. This paper considers the diffraction of plane incident waves on a floating flexible ring-shaped plate and its response to the incident waves. An analytic and numerical study of the hydroelastic behavior of the plate is presented. An integro-differential equation is derived for the problem and an algorithm of its numerical solution is proposed. The representation of the solution as a series of Hankel functions is the key ingredient of the approach. The problem is first formulated. The main integro-differential equation is derived on the basis of the Laplace equation and thin-plate theory. The free-surface elevation, plate deflection and Green's function are expressed in polar coordinates as superpositions of Hankel and Bessel functions, respectively. These expressions are used in a further analysis of the integro-differential equation. The problem is solved for two cases of water depth: infinite and finite. For the coefficients in the case of infinite depth a set of algebraic equations is obtained, yielding an approximate solution. Then a solution is obtained for the general and most interesting case of finite water depth analogously in the seventh section. The exact solution might be approximated by taking into account a finite number of the roots of the plate dispersion relation. Also, the influence of the plate's motion on wave propagation in the open water field and within the gap of the ring is studied. Numerical results are presented for illustrative purposes.

Key words: diffraction, hydroelastic response, integro-differential equation, plate-water interaction, ring-shaped plate

Abbreviations: VLFP – very large floating platform, IWD – infinite water depth, FWD – finite water depth, IDE – integro-differential equation.

1. Introduction and background

This paper considers the hydroelastic behavior of a floating elastic plate and its response to the incident surface water waves. A thin plate with elastic properties serves as a model for a very large floating platform (VLFP) designed for the purpose of an airport, ferry pier or other artificial construction, floating in offshore zone. VLFPs have a mat-like dynamic behavior which can be described by the plate motion equation. As the horizontal dimensions of VLFP are about several kilometers by several hundred meters, while the thickness and draft are of order of several meters, it is possible to consider the platform as a thin plate, using one of the standard theories of Kirchhoff, Timoshenko or Mindlin. Such a plate can also serve as a model of a huge ice field for studying ice-water interaction. Water depth plays an important role; therefore, the theory is divided into three cases: very deep water (depth assumed to be infinite), water of finite depth, and shallow water.

There are many papers considering plate-water interaction. For this problem a very detailed literature survey has recently been published by Watanabe *et al.* [1]. Mainly plates of rectangular platforms were studied, while there are very few papers considering arbitrarily shaped VLFPs. Several papers, studying the circular plate, have been published recently. The problem for the circular plate for shallow water was solved by Zilman and Miloh [2] and

Tsubogo [3]. For finite water depth the problem was solved by Watanabe *et al.* [4] by use of the Galerkin method and Mindlin plate theory, and Peter *et al.* [5] who presented a solution based on decomposing the deflection into angular eigenfunctions. Andrianov and Hermans [6] solved the problem of the circular disk for water of finite and infinite depth, using an integro-differential formulation.

Here we extend the theory to the case of a ring-shaped plate (or, as in some of the literature, a circular plate with a circular hole). The floating structure of this form may be either of large dimension, for purposes of VLFP, or small, for other purposes. The hydroelastic behavior of the ring-shaped floating elastic plate and its response to incident surface waves are investigated. The ring floats on the surface of ideal, incompressible fluid. We consider two cases of water depth. First, we study the behavior of the ring floating on the surface of water of infinite depth. Next, the case of water of finite depth is considered, where the general analysis and set of equations are more complicated as more roots of a water dispersion relation have to be taken into account. An analytical study is carried out and presented for both cases. The problem for water of shallow depth can be solved more easily by the use of well-known Stoker approximation theory. In the latter case a set of equations is derived from free-edge and transition conditions at the inner and outer edges of the ring.

An integro-differential formulation, which allows us to solve the diffraction problem for different geometrical configurations, was developed and applied in [6–9]. This formulation might be applied to a plate of finite or infinite dimensions and even to the case of multiple plates. Also the thin plate theory, standard Laplace equation in the fluid, supplemented by surface and boundary conditions, and Green's theorem are used.

We consider a plate having elastic properties of constant flexural rigidity and homogeneous stiffness. The edges of the ring are free of shear forces, bending and twisting moments. The plate deflection is generated by incoming plane surface waves. The solution for the plate deflection and free-surface elevation in the far field and ring gap is derived. The plate deflection is represented as a superposition of Hankel functions with corresponding coefficients, containing amplitudes. In a similar way, we represent the Green's function, obeying the boundary conditions at the free surface, as a series of Bessel functions for both cases of water depth. Next, Graf's addition theorem is applied to the Green's function.

Further, we derive the governing integro-differential equation. The problem involves two dispersion relations: one in the plate region and the other in the open water. An analysis of integrals in the complex plane and use of Cauchy's theorem and the Wronskian lead us to the dispersion relation in the plate region. Furthermore, we derive from the integro-differential equation, supplemented by the free-edge conditions, a set of equations for the coefficients in the series expansion to determine the plate deflection. Also, we study the free-surface elevation in the ring gap and in the open water field. To analyze the influence of the presence of the plate on the propagation of the incoming waves, results are obtained for the wave pattern generated by the plate's motion. Numerical results for the plate deflection and the free-surface elevation are obtained for different values of the physical parameters.

2. Mathematical formulation

A floating thin elastic ring-shaped plate of inner radius r_1 and outer radius r_0 covers a part of the surface of an ideal, incompressible expanse of water. The plate with zero thickness can serve as a model of the VLFP, as described above, due to the small thickness and shallow draft of the platform. The water depth h is infinite for the case of deep water and finite and

constant for the other case. We assume that no space exists between the free surface and the plate. The flexural rigidity of the thin elastic isotropic plate is constant.

The plate deflection is generated by incoming surface waves of length λ. It is also assumed that incoming waves are propagating in water that is still homogeneous in the positive x-direction. The wave amplitude A is rather small in comparison with other length-parameters of the problem.

The horizontal geometry sketch of the plate is shown in Figure 1. The radial coordinate ρ is measured from the centre of the plate. We denote the surface of the fluid domain in the plate region ($r_1 \le \rho \le r_0$) as $\mathcal{P}$ and in the open water as $\mathcal{F}$, where the open-water region outside the plate is $\mathcal{F}_0$ ($\rho > r_0$) and the gap area $\mathcal{F}_1$ ($\rho < r_1$). Three-dimensional Laplacian is

$$\Delta = \nabla^2 = \frac{\partial^2}{\partial \rho^2} + \frac{1}{\rho}\frac{\partial}{\partial \rho} + \frac{1}{\rho^2}\frac{\partial^2}{\partial \varphi^2} + \frac{\partial^2}{\partial z^2}$$

in polar coordinates, while their relations to Cartesian coordinates are the following: $\rho^2 = x^2 + y^2$, $\varphi = \arctan y/x$, $z = z$.

The velocity potential is introduced by $\nabla\Phi(\boldsymbol{\rho}, t) = \mathbf{V}(\boldsymbol{\rho}, t)$, where $\mathbf{V}(\boldsymbol{\rho}, t)$ is the fluid velocity vector. The velocity potential $\Phi(\boldsymbol{\rho}, t)$ is a solution of the governing Laplace equation in the fluid

$$\Delta\Phi = 0, \tag{1}$$

for $z < 0$ in the case of infinite water depth (IWD) or $-h < z < 0$ for finite water depth (FWD), supplemented by the boundary conditions at the free surface and at the bottom. The linearized kinematic condition in the plate and water regions, at the surface $z = 0$, has the form

$$\frac{\partial\Phi}{\partial z} = \frac{\partial w}{\partial t}, \tag{2}$$

where $w(\rho, \varphi, t)$ denotes either the free-surface elevation or the deflection of the plate; t is the time. Later, to distinguish the vertical displacements, we denote the free-surface elevation in the open water region $\mathcal{F}$ by ζ, while the plate deflection in $\mathcal{P}$ is still denoted by w. The dynamic condition, derived from the linearized Bernoulli equation, has the form

$$\frac{P - P_{\text{atm}}}{\rho_{\text{w}}} = -\frac{\partial\Phi}{\partial t} - gw, \tag{3}$$

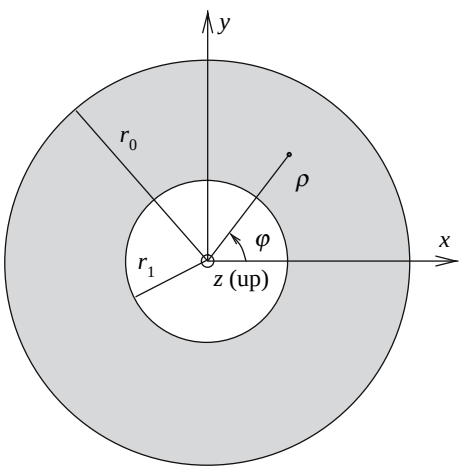

Figure 1. Geometry and coordinate system of the problem.

at $z=0$, where ρ_w is the density of the water, g is the gravitational acceleration, $P(\rho,\varphi,t)$ is the pressure in the fluid, and P_{atm} is the atmospheric pressure. Relations (2–3) are the kinematic and dynamic conditions at the free surface. The linearized free-surface condition in the water region $\mathcal{F}$ takes the form

$$\frac{\partial\Phi}{\partial z}=-\frac{1}{g}\frac{\partial^2\Phi}{\partial t^2} \tag{4}$$

at $z=0$. The other boundary condition at the bottom $z=-h$, applying to the case of finite depth, is written in the following form

$$\frac{\partial\Phi}{\partial z}=0. \tag{5}$$

The edges of the ring are free of vertical shear forces, bending and twisting moments. Therefore, the free-edge conditions at $\rho=r_1$ and $\rho=r_0$ are:

$$\left\{\nabla^2-\frac{(1-\nu)}{\rho}\left(\frac{\partial}{\partial\rho}+\frac{1}{\rho}\frac{\partial^2}{\partial\varphi^2}\right)\right\}w=0, \tag{6}$$

$$\left\{\frac{\partial}{\partial\rho}\nabla^2+\frac{(1-\nu)}{\rho^2}\left(\frac{\partial}{\partial\rho}-\frac{1}{\rho}\right)\frac{\partial^2}{\partial\varphi^2}\right\}w=0, \tag{7}$$

where ν is the Poisson ratio. Here and in the sequel the Laplacian is two-dimensional, except when the Green's function is derived.

3. Integro-differential equation

In this section the main integro-differential equation (IDE) is derived along the plate contour, consisting of the inner and outer edges of the ring. We use the approach described and applied in [7,8] for plates of rectangular shape in Cartesian coordinates. The derivation of IDE in polar coordinates has recently been published by the authors [6].

To describe the deflection of the plate w we apply the isotropic thin-plate theory, see, *e.g.*, [10], which leads to a differential equation at $z=0$ in the plate area $\mathcal{P}$, known as the Gehring-Kirchhoff equation

$$D\Delta^2 w+m\frac{\partial^2 w}{\partial t^2}=P-P_{atm}, \tag{8}$$

where m is the mass of a unit area of the plate, D is the flexural rigidity, expressed in terms of Young's modulus E, Poisson ratio ν and the plate thickness h_p:

$$D=\frac{Eh_p^3}{12(1-\nu^2)}\ .$$

For both IWD and FWD cases, we apply the operator $\partial/\partial t$ to (8) and use the surface conditions (2) and (3) to arrive at the following equation for the total potential Φ

$$\left(\frac{D}{\rho_w g}\Delta^2+\frac{m}{\rho_w g}\frac{\partial^2}{\partial t^2}+1\right)\frac{\partial\Phi}{\partial z}+\frac{1}{g}\frac{\partial^2\Phi}{\partial t^2}=0. \tag{9}$$

With the usual assumptions of an ideal fluid and small wave amplitude, the potential can be written in the form $\Phi(\rho,\varphi,z,t)=\phi(\rho,\varphi,z)e^{-i\omega t}$, where ω is the wave frequency; this means we consider harmonic waves. From (2) it follows that the surface elevation has the same harmonic behavior, whence we have the functions $w(\rho,\varphi)$ and $\zeta(\rho,\varphi)$ in $\mathcal{P}$ and $\mathcal{F}$,

respectively. Thus, we consider waves of the single frequency ω and obtain the following differential equation for the potential ϕ at $z=0$

$$\left(\mathcal{D}\Delta^2-\mu+1\right)\frac{\partial\phi}{\partial z}-K\phi=0, \tag{10}$$

where $\mathcal{D}=D/\rho_w g$, $\mu=m\omega^2/\rho_w g$ are additional physical parameters that are constant as the plate considered is isotropic, and $K=\omega^2/g$.

The potential of the undisturbed incident wave ϕ^{inc}, in polar coordinates, is

$$\phi^{inc}(\rho,\varphi,z)=\begin{cases}\dfrac{gA}{i\omega}e^{ik_0\rho\cos\varphi+k_0 z} & \text{for IWD,}\\[2ex] \dfrac{\cosh k_0(z+h)}{\cosh k_0 h}\dfrac{gA}{i\omega}e^{ik_0\rho\cos\varphi} & \text{for FWD,}\end{cases} \tag{11}$$

where A is the amplitude of the incident wave, and k_0 is the wave number. The wave height is defined as twice the amplitude. For deep water the wave number is $k_0=K$ and for water of finite depth the wave number k_0 is the positive real solution of the water dispersion relation

$$k\tanh kh=K. \tag{12}$$

The length of the incoming waves is $\lambda=2\pi/k_0$. Normally, in a practical situation the outer diameter $2r_0$ of the ring-shaped VLFP is longer than the wave length; the reverse case corresponds to extremely long waves.

The potential must satisfy the Sommerfeld radiation condition

$$\sqrt{\rho}\left(\frac{\partial}{\partial\rho}-ik_0\right)\left(\phi-\phi^{inc}\right)=0 \tag{13}$$

when $\rho\to\infty$.

The free-surface elevation ζ in the open water $\mathcal{F}$ equals to the sum of the incident wave elevation ζ^{inc}, and the additional wave elevation ζ^{pm}, generated by the plate motion

$$\zeta=\zeta^{inc}+\zeta^{pm}. \tag{14}$$

The total potential in $\mathcal{F}$ is also represented as the sum of the incident wave potential and the potential of waves arising because of the motion of the plate

$$\phi^{\mathcal{F}}=\phi^{inc}+\phi^{pm}, \tag{15}$$

where ϕ^{pm} is the diffraction potential plus the radiation potential. In fact, the potential ϕ^{pm} must satisfy radiation condition (13). The governing equations for the regions $\mathcal{F}_0$ and $\mathcal{F}_1$ are the same; due to the fact that $\rho>r_0$ and $\rho<r_1$, respectively, differences in the analysis will appear, which will be discussed later.

We introduce the Green's function $\mathcal{G}(r,\theta;\rho,\varphi)$, fullfilling the free-surface and the radiation conditions, and apply Green's theorem to the potentials in the water and plate regions $\phi^{\mathcal{F}}$ and $\phi^{\mathcal{P}}$, respectively. Analyzing the obtained relations and using the dynamic (10) and kinematic (2) conditions, we obtain the main integro-differential equation in general form at the free surface $z=0$

$$\left\{\mathcal{D}\Delta^2-\mu+1\right\}w(\rho,\varphi)=\frac{K}{4\pi}\int\limits_{\mathcal{P}}\left\{\mathcal{D}\Delta^2-\mu\right\}\mathcal{G}(r,\theta;\rho,\varphi)w(r,\theta)\,r\,dr\,d\theta+Ae^{ik_0\rho\cos\varphi}, \tag{16}$$

where the last term represents the potential of the incoming waves. The presented derivation of IDE can be done in polar and Cartesian coordinates, *i.e.*, for plates of any geometrical shape. Detailed information on the derivation of IDE is given in [6] for polar coordinates and in [7–8] for Cartesian coordinates.

4. Green's function and deflection

In this section we describe the Green's function, plate deflection and the operations on corresponding Bessel and Hankel functions for the ring-shaped plate. The general expressions for the Green's function of a surface singularity for water of infinite and finite depth can be found in [11]. The description of the modified Green's function, which is used in this paper, was published by the authors in [6].

We introduce the Green's function for a source within the fluid that in Cartesian coordinates fulfills $\Delta\mathcal{G} = 4\pi\delta(\mathbf{x} - \boldsymbol{\xi})$, where δ is the Dirac δ-function, $\mathbf{x}$ is a source point and $\boldsymbol{\xi}$ is an observation point. The Green's function obeys the boundary conditions at the free surface, $\mathcal{G}_z = K\mathcal{G}$, and at the bottom (for FWD) as well as the radiation condition. The three-dimensional Green's function at $z = \zeta = 0$ takes the following form [6]

$$\mathcal{G}(x, y; \xi, \eta) = -2\int_{\mathcal{L}} F(k)\mathrm{J}_0(kR)\,\mathrm{d}k, \tag{17}$$

where $\mathrm{J}_0(kR)$ is the Bessel function, R measures horizontal distance, *viz.* $R^2 = (x-\xi)^2 + (y-\eta)^2$ in Cartesian coordinates. $\mathcal{L}$ is the integration contour in the complex k-plane from 0 to $+\infty$, passing beneath the singularity $k = k_0$, as shown in Figure 2, and chosen such that the radiation condition is satisfied. The function $F(k)$ in (17) is given by

$$F(k) = \begin{cases} \dfrac{k}{k - k_0} & \text{for IWD,} \quad \text{(a)} \\ \dfrac{k\cosh kh}{k\sinh kh - K\cosh kh} & \text{for FWD,} \quad \text{(b).} \end{cases} \tag{18}$$

In the FWD case we have additional poles $k = \pm k_i$ on the imaginary axis of the complex plane.

The horizontal distance R in polar coordinates is written as $R^2(\rho, \varphi; r, \theta) = \rho^2 + r^2 - 2\rho r\cos(\theta - \varphi)$. Here ρ and r are the distances from the center of the plate to the source and observation points, respectively, and $\theta - \varphi$ is the angle between r and ρ.

If we apply Graf's addition theorem to the Bessel function $\mathrm{J}_0(kR)$, which is also called Neumann's formula for the Bessel function of order zero, it can be replaced by the series [12]

$$\mathrm{J}_0(kR) = \sum_{q=0}^{\infty} \delta_q \mathrm{J}_q(kr)\mathrm{J}_q(k\rho)\cos q(\theta - \varphi), \tag{19}$$

where $\delta_0 = 1$ and $\delta_q = 2$ if $q > 0$. We truncate the series in (19) at $q = N$, chosen such that convergence of the final results is guaranteed, taking into account the decaying behavior of the Bessel functions with respect to the order. The value of N is chosen later; all terms of

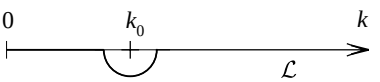

Figure 2. Contour of the integration.

order higher than N are negligibly small. This is justified by invoking a computational test. The Green's function in polar coordinates now takes the form

$$\mathcal{G}(r,\theta;\rho,\varphi) = -2\int_{\mathcal{L}} F(k)\sum_{q=0}^{N}\delta_q \mathrm{J}_q(kr)\mathrm{J}_q(k\rho)\cos q(\theta-\varphi)\,\mathrm{d}k. \tag{20}$$

In the sequel, we use the Green's function in the form (20).

At the same time the deflection function has to be chosen for each shape of the plate separately. For the circular plate it can be expressed by the superposition of Bessel functions [6]. Analogously, for the ring-shaped plate the deflection can be represented as a series of Hankel functions with corresponding coefficients of the following form

$$w(\rho,\varphi) = \sum_{m=1}^{M}\sum_{n=0}^{N}\left[a_{mn}^{(1)}\mathrm{H}_n^{(1)}(\kappa_m\rho) + a_{mn}^{(2)}\mathrm{H}_n^{(2)}(\kappa_m\rho)\right]\cos n\varphi, \tag{21}$$

where $a_{mn}^{(1)}$ and $a_{mn}^{(2)}$ are unknown amplitude functions, κ_m are the roots of the plate dispersion relation, which are the so-called reduced wave numbers, and M is the number of these roots taken into account in the computations.

For the IWD case we use three roots of the dispersion relation in the plate area

$$\left(\mathcal{D}\kappa^4 - \mu + 1\right)\kappa = \pm k_0. \tag{22}$$

The roots of the plate dispersion relation (22), shown in Figure 3, are the following: two real roots $\pm\kappa_1$, and four complex roots $\pm\kappa_2$ and $\pm\kappa_3$, which are symmetrically placed with respect to both the real and imaginary axes. Due to a property of Hankel functions, three roots are taken into account for the current situation: real positive κ_1 and roots κ_2 and κ_3, with equal imaginary parts and equal, but opposite-signed real parts, all three being located in the upper half-plane. The real root κ_1 represents the main traveling wave mode, the two complex roots represent damped wave modes.

The plate dispersion relation for water of finite depth has the following form

$$\left(\mathcal{D}\kappa^4 - \mu + 1\right)\kappa\tanh\kappa h = K. \tag{23}$$

The dispersion relation (23) has two real roots $\pm\kappa_1$, and four complex roots $\pm\kappa_2$ and $\pm\kappa_3$ symmetrically placed with respect to both the real and imaginary axes, these six being of the same order as in the IWD case, and infinitely many purely imaginary roots. We take into account M roots of Equation (23): one real positive κ_1, two complex roots κ_2 and κ_3, having equal imaginary parts and equal but opposite-signed real parts, and $M-3$ imaginary roots, all located in the upper half-plane.

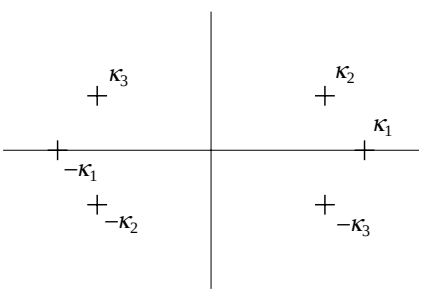

Figure 3. Zeros of the dispersion relation for deep water.

The positions of the roots κ_m in the complex k-plane are similar to those of the roots of the water dispersion relation (12), which has one real root k_0, corresponding to only one wave number of deep water, and a number of purely imaginary roots k_i, $i=1,\ldots,M-3$, except for two complex roots κ_2 and κ_3. Thus, in the FWD case M is the truncation parameter, and we take into account M roots of the plate dispersion relation (23) κ_m, $m=1,\ldots,M$, and $M-2$ roots of the water dispersion relation (12) k_i, $i=0,\ldots,M-3$.

5. Set of equations

At this point we have only equations resulting from the free-edge conditions to determine the unknown amplitudes $a_{mn}^{(1)}$ and $a_{mn}^{(2)}$. Next we will derive relations from the integro-differential equation to complete the set of equations.

If we insert the relations for the deflection (21) and Green's function (20) into (16), the integro-differential equation at the free surface $z=0$ takes the expanded form

$$\begin{aligned}
&\left\{\mathcal{D}\Delta^2-\mu+1\right\}\sum_{m=1}^{M}\left[\sum_{n=0}^{N}a_{mn}^{(1)}\mathrm{H}_n^{(1)}(\kappa_m\rho)\cos n\varphi+\sum_{n=0}^{N}a_{mn}^{(2)}\mathrm{H}_n^{(2)}(\kappa_m\rho)\cos n\varphi\right]\\
&\quad+\frac{K}{2\pi}\int_0^{2\pi}\int_{r_1}^{r_0}\left\{\mathcal{D}\Delta^2-\mu\right\}\sum_{m=1}^{M}\left[\sum_{n=0}^{N}a_{mn}^{(1)}\mathrm{H}_n^{(1)}(\kappa_m r)\cos n\theta+\sum_{n=0}^{N}a_{mn}^{(2)}\mathrm{H}_n^{(2)}(\kappa_m r)\cos n\theta\right]\\
&\quad\times\int_{\mathcal{L}}F(k)\sum_{q=0}^{N}\delta_q\mathrm{J}_q(kr)\mathrm{J}_q(k\rho)\cos q(\theta-\varphi)\,\mathrm{d}k\,r\,\mathrm{d}r\,\mathrm{d}\theta=A\sum_{n=0}^{N}\epsilon_n\mathrm{J}_n(k_0\rho)\cos n\varphi,
\end{aligned}\tag{24}$$

where $\epsilon_n=\delta_n\mathrm{i}^n$. Due to the orthogonality relation for the cosine function, we only get a non-zero contribution in the integrand for $n=q$. Next we carry out the integration with respect to θ in (24). The integration over θ itself, when only components dependent on θ are considered, gives 2π for $n=0$ and $\delta_n\pi\cos n\varphi$ for $n>0$, which means $2\pi\cos n\varphi$ for all n. Then, using the orthogonality of the cosine function, we end up with the following set of $N+1$ equations derived from IDE (24):

$$\begin{aligned}
&\sum_{m=1}^{M}\left(\mathcal{D}\kappa_m^4-\mu+1\right)\left[a_{mn}^{(1)}\mathrm{H}_n^{(1)}(\kappa_m\rho)+a_{mn}^{(2)}\mathrm{H}_n^{(2)}(\kappa_m\rho)\right]\\
&\quad+K\int_{r_1}^{r_0}\sum_{m=1}^{M}\left(\mathcal{D}\kappa_m^4-\mu\right)\left[a_{mn}^{(1)}\mathrm{H}_n^{(1)}(\kappa_m r)+a_{mn}^{(2)}\mathrm{H}_n^{(2)}(\kappa_m r)\right]\\
&\quad\times\int_{\mathcal{L}}F(k)\mathrm{J}_n(kr)\mathrm{J}_n(k\rho)\,\mathrm{d}k\,r\,\mathrm{d}r=A\epsilon_n\mathrm{J}_n(k_0\rho),
\end{aligned}\tag{25}$$

for $n=0,\ldots,N$. In accordance with [13, Equation 21.8–22] the integration with respect to r leads us to the difference of two Lommel integrals at r_0 and r_1. Equation (25) takes the form

$$\begin{aligned}
&\sum_{m=1}^{M}\left(\mathcal{D}\kappa_m^4-\mu+1\right)\left[a_{mn}^{(1)}\mathrm{H}_n^{(1)}(\kappa_m\rho)+a_{mn}^{(2)}\mathrm{H}_n^{(2)}(\kappa_m\rho)\right]\\
&\quad+K\int_{\mathcal{L}}\sum_{m=1}^{M}\left(\mathcal{D}\kappa_m^4-\mu\right)\frac{F(k)}{(k^2-\kappa_m^2)}\left[a_{mn}^{(1)}c_{mn}^{(1)}+a_{mn}^{(2)}c_{mn}^{(2)}\right]\mathrm{J}_n(k\rho)\,\mathrm{d}k=A\epsilon_n\mathrm{J}_n(k_0\rho),
\end{aligned}\tag{26}$$

where we have introduced the function $c_{mn}^{(q)}$ as a combination of Bessel and Hankel functions in the form

$$c_{mn}^{(q)} = r_0\left[k\mathrm{J}_{n+1}(kr_0)\mathrm{H}_n^{(q)}(\kappa_m r_0) - \kappa_m \mathrm{J}_n(kr_0)\mathrm{H}_{n+1}^{(q)}(\kappa_m r_0)\right] - r_1\left[k\mathrm{J}_{n+1}(kr_1)\mathrm{H}_n^{(q)}(\kappa_m r_1) - \kappa_m \mathrm{J}_n(kr_1)\mathrm{H}_{n+1}^{(q)}(\kappa_m r_1)\right], \quad q = 1, 2. \tag{27}$$

From Equation (26) we can derive $2(M-2)(N+1)$ relations for the determination of $2M(N+1)$ unknown amplitudes. The set of equations for both cases of water depth is completed by the free-edge conditions (6) and (7) when the deflection function is inserted there. These conditions at the edges $\rho = r_1$ and $\rho = r_0$ give us $4(N+1)$ equations

$$\sum_{m=1}^{M} a_{mn}^{(1)} d_{mn,ij}^{(1)} + a_{mn}^{(2)} d_{mn,ij}^{(2)} = 0, \tag{28}$$

where $n = 0, \ldots, N$, $i = 0, 1$, $j = 1, 2$, and the functions $d_{mn,ij}^{(q)}$ are

$$d_{mn,i1}^{(q)} = \left[\mathrm{H}_n^{(q)}(\kappa_m r_i)\left(-\kappa_m^2 + \frac{(1-\nu)n(n-1)}{r_i^2}\right) + \mathrm{H}_{n+1}^{(q)}(\kappa_m r_i)\kappa_m \frac{(1-\nu)}{r_i}\right],$$
$$d_{mn,i2}^{(q)} = \left[\mathrm{H}_n^{(q)}(\kappa_m r_i)\left(-\frac{n}{r_i}\kappa_m^2 + \frac{(1-\nu)n^2(1-n)}{r_i^3}\right) + \mathrm{H}_{n+1}^{(q)}(\kappa_m r_i)\left(\kappa_m^3 + \frac{(1-\nu)n^2}{r_i^2}\kappa_m\right)\right], \tag{29}$$

where $q = 1, 2$ is the Hankel-function index and r_i is either inner-ring contour r_1 or outer-ring contour r_0.

From now on we consider the IWD and FWD cases separately.

6. Ring on water of infinite depth

Here the analytic study is given for the case of infinite depth. In the IWD case we only consider part of the solution, namely that related to the water dispersion relation. The analysis given in this section is a good basis from which to derive a solution for the general and most complicated case of water of finite depth. To demonstrate the method we wish to use for the FWD case, we consider the contribution of the pole $k = k_0$ in the IWD case. Here we ignore the contribution of the integral along the imaginary axis after closing the contour in (20). This means that local disturbances are disregarded.

The deflection of the plate, the Green's function and the function $F(k)$ are represented by expressions (21), (20) and (18a), respectively. For deep-water wave number k_0 equals K, so $k_0 = \omega^2/g$.

Now we analyze the k-integral in IDE (26). The integrand has the poles $k = \pm\kappa_m$, shown in Figure 3, and can be represented as a sum of four integrals

$$k_0 \int_0^{\infty} \frac{k}{(k-k_0)(k^2-\kappa_m^2)}\left[a_{mn}^{(1)}c_{mn}^{(1)} + a_{mn}^{(2)}c_{mn}^{(2)}\right]\mathrm{J}_n(k\rho)\,\mathrm{d}k = a_{mn}^{(1)}(I_{01} - I_{11}) + a_{mn}^{(2)}(I_{02} - I_{12}), \tag{30}$$

where the path of integration in (31) is below the singularities $k = k_0$ and $k = \kappa_1$, respectively, and the integrals I_{iq} for $i = 0, 1$, $q = 1, 2$ are

$$I_{iq} = k_0 r_i \int_0^{\infty} \frac{k}{(k-k_0)(k^2-\kappa_m^2)}\left[k\mathrm{J}_{n+1}(kr_i)\mathrm{H}_n^{(q)}(\kappa_m r_i) - \kappa_m \mathrm{J}_n(kr_i)\mathrm{H}_{n+1}^{(q)}(\kappa_m r_i)\right]\mathrm{J}_n(k\rho)\mathrm{d}k, \tag{31}$$

with r_i as r_1 or r_0, $m=1,\ldots,M$ and $n=0,\ldots,N$. The contour of integration may be closed in the complex k-plane. In the integral I_{iq} we split up the Bessel function of largest argument to be able to close the contour of integration and, furthermore, use Jordan's lemma.

Let us consider the integral I_{01}. For further manipulation we use the fact that $\rho < r_0$ and then the Bessel function $\mathrm{J}_t(kr_0)$ is written as the half-sum of the corresponding Hankel functions of the first and second kind

$$\mathrm{J}_t(kr_0)=\frac{\mathrm{H}_t^{(1)}(kr_0)+\mathrm{H}_t^{(2)}(kr_0)}{2}, \tag{32}$$

where t is n or $n+1$. Then I_{01} is decomposed into two integrals. Those two we transform into integrals along the vertical axis in the complex k-plane plus the sums of the residues at the poles with factors $2\pi\mathrm{i}$ as shown in Figure 3. Then the contour of integration for the first integral with $\mathrm{H}_t^{(1)}(kr_0)$ is closed in the upper half-plane with the poles $k=\kappa_m$, and for the second one with $\mathrm{H}_t^{(2)}(kr_0)$ is closed in the lower half-plane, where the poles are at $k=-\kappa_m$. These two situations have to be considered separately.

If we apply the same procedure to the integral I_{02}, the contour for its first integral, obtained by (32) and containing $\mathrm{H}_t^{(1)}(kr_0)$, can be closed in the upper half-plane, and for the integral with $\mathrm{H}_t^{(2)}(kr_0)$ in the lower half-plane. For the integrals I_{11} and I_{12} the same closure procedure is applied, but with one sufficient difference. In this case $\rho > r_1$ and, therefore, to close the contours of integration we represent the Bessel functions $\mathrm{J}_n(k\rho)$ as the half-sums of corresponding Hankel functions of the first and second kind, as was done in (32).

When the contours are closed for all integrals, we apply the Cauchy residue lemma at the poles $k=\kappa_m$ for the integrals with the contour closed in the upper half-plane and at the poles $k=-\kappa_m$ for the integrals with the contour closed in the lower half-plane. The Wronskian $W\{\mathrm{H}_n^{(1)}(\kappa_m r_i), \mathrm{H}_n^{(2)}(\kappa_m r_i)\}$ applies for the combination of Hankel functions

$$\mathrm{H}_{n+1}^{(1)}(\kappa_m r_i)\mathrm{H}_n^{(2)}(\kappa_m r_i)-\mathrm{H}_n^{(1)}(\kappa_m r_i)\mathrm{H}_{n+1}^{(2)}(\kappa_m r_i)=-\frac{4\mathrm{i}}{\pi\kappa_m r_i}. \tag{33}$$

Then, adding up the resulting terms and considering the coefficients of $\mathrm{J}_n(\kappa r_i)$, we derive the plate dispersion relation for deep water (22), where the plus sign in the right-hand side corresponds to the integrals in the upper half-plane, and the minus sign to the integrals in the lower half-plane. The derivation of the plate dispersion relation from IDE is also a justification of our approach.

In the upper half-plane we also obtain a contribution of the pole $k=k_0$ of the integrand, as seen in Figure 2. This contribution has to cancel the term in the right-hand side of IDE (26). If we neglect the integral along the imaginary axis, application of Jordan's lemma and the contribution of the pole $k=k_0$ lead us to $2(N+1)$ relations

$$\pi\mathrm{i}r_0\sum_{m=1}^{M}\left(\mathcal{D}\kappa_m^4-\mu\right)\frac{k_0^2}{k_0^2-\kappa_m^2}\Big[k_0\mathrm{H}_{n+1}^{(1)}(k_0r_0)\left(a_{mn}^{(1)}\mathrm{H}_n^{(1)}(\kappa_m r_0)+a_{mn}^{(2)}\mathrm{H}_n^{(2)}(\kappa_m r_0)\right) -\kappa_m\mathrm{H}_n^{(1)}(k_0r_0)\left(a_{mn}^{(1)}\mathrm{H}_{n+1}^{(1)}(\kappa_m r_0)+a_{mn}^{(2)}\mathrm{H}_{n+1}^{(2)}(\kappa_m r_0)\right)\Big]=A\epsilon_n \tag{34}$$

and

$$\pi\mathrm{i}r_1\sum_{m=1}^{M}\left(\mathcal{D}\kappa_m^4-\mu\right)\frac{k_0^2}{k_0^2-\kappa_m^2}\Big[k_0\mathrm{J}_{n+1}(k_0r_1)\left(a_{mn}^{(1)}\mathrm{H}_n^{(1)}(\kappa_m r_1)+a_{mn}^{(2)}\mathrm{H}_n^{(2)}(\kappa_m r_1)\right) -\kappa_m\mathrm{J}_n(k_0r_1)\left(a_{mn}^{(1)}\mathrm{H}_{n+1}^{(1)}(\kappa_m r_1)+a_{mn}^{(2)}\mathrm{H}_{n+1}^{(2)}(\kappa_m r_1)\right)\Big]=0. \tag{35}$$

We have now derived a system of $2M(N+1)$ equations (34–35) and (28) with $M=3$ for the determination of $6(N+1)$ amplitudes $a_{mn}^{(1)}$ and $a_{mn}^{(2)}$ for 'infinitely' deep water. When the amplitudes are known, the plate deflection is calculated by (21).

7. Ring on water of finite depth

In this section we consider a ring on water of finite depth. In general we follow the analysis as presented in the previous section for the IWD case. For the FWD case the deflection of the plate is represented by (21) and the Green's function is given by formulas (20) and (18b). Here we take into account $M-2$ roots of the water dispersion relation (12) and M roots of the plate dispersion relation (23).

Let us consider the function $F(k)$ given by (18b). For the FWD case this function is meromorphic, as it is bounded for all poles. The poles are the roots of the dispersion relation for the water region (12) $k=\pm k_i$, $i=0,\ldots,M-3$, where k_0 is the positive real root and k_i, for $i\neq 0$, is the purely imaginary. Thus, the meromorphic function $F(k)$ for water of finite depth can be expressed by the following relation

$$F(k)=\sum_{i=0}^{M-3}\frac{k_i^2}{k_i^2h-K^2h+K}\left(\frac{1}{k+k_i}+\frac{1}{k-k_i}\right). \tag{36}$$

The relation (36) is inserted into IDE (26). There are two integrals in the complex k-plane, those two can be combined into one integral from $-\infty$ to $+\infty$ with the poles $k=k_i$. The contour of integration is defined as $\mathcal{L}'$. Finally, we derive the governing integro-differential equation for the case of finite water depth

$$\sum_{m=1}^{M}\left(\mathcal{D}\kappa_m^4-\mu+1\right)\left[a_{mn}^{(1)}\mathrm{H}_n^{(1)}(\kappa_m\rho)+a_{mn}^{(2)}\mathrm{H}_n^{(2)}(\kappa_m\rho)\right]+K\int_{\mathcal{L}'}\sum_{m=1}^{M}\left(\mathcal{D}\kappa_m^4-\mu\right)$$
$$\times\frac{\mathrm{J}_n(k\rho)}{(k^2-\kappa_m^2)}\sum_{i=0}^{M-3}\frac{k_i^2}{(k_i^2h-K^2h+K)(k-k_i)}\left[a_{mn}^{(1)}c_{mn}^{(1)}+a_{mn}^{(2)}c_{mn}^{(2)}\right]\mathrm{d}k=A\epsilon_n\mathrm{J}_n(k_0\rho) \tag{37}$$

at $z=0$, where $n=0,\ldots,N$ and the functions $c_{mn}^{(q)}$ are given by (27) for $q=1,2$.

To obtain the dispersion relation we repeat the procedure that was applied for the IWD case: the representation of k-integral as a sum of four integrals and, further, decomposition of each of those four into two integrals with contours closed in the different half-planes of the complex plane. In the FWD case we have the poles, given in Figure 3, plus the poles at the imaginary axis $\pm\kappa_m$ for $m=4,\ldots,M$. The application of the residue lemma at the poles leads us to the standard plate dispersion relation for water of finite depth (23).

Next we consider the contributions of the poles of the water dispersion relation (12). The closure of the contour is shown in Figure 4. The contour for the integrals with $\mathrm{H}_q^{(1)}(kr_i)$ might be closed in the upper half-plane, while the contour for the integrals with $\mathrm{H}_q^{(2)}(kr_i)$ in the lower half-plane. In the latter case we get a zero contribution because the poles $k=k_i$ are located as indicated in Figure 4.

An application of the Cauchy theorem to the integrals with the contour closed in the upper half-plane gives us equations to determine the amplitudes $a_{mn}^{(1)}$ and $a_{mn}^{(2)}$. The poles $k=k_i$, where $i=0,\ldots,M-3$, result in $2(M-2)(N+1)$ equations. First $(M-2)(N+1)$ equations

are derived along the outer ring edge $\rho = r_0$ and have the following form

$$\pi \mathrm{i} K r_0 \sum_{m=1}^{M} \frac{\left(\mathcal{D}\kappa_m^4 - \mu\right) k_i^2}{(k_i^2 - \kappa_m^2)(k_i^2 h - K^2 h + K)} \times \Big[k_i \mathrm{H}_{n+1}^{(1)}(k_i r_0) \left(a_{mn}^{(1)} \mathrm{H}_n^{(1)}(\kappa_m r_0) + a_{mn}^{(2)} \mathrm{H}_n^{(2)}(\kappa_m r_0) \right) - \kappa_m \mathrm{H}_n^{(1)}(k_i r_0) \left(a_{mn}^{(1)} \mathrm{H}_{n+1}^{(1)}(\kappa_m r_0) + a_{mn}^{(2)} \mathrm{H}_{n+1}^{(2)}(\kappa_m r_0) \right) \Big] = A_i, \tag{38}$$

where

$$A_i = \begin{cases} A\epsilon_n, & i = 0, \\ 0, & i = 1, \ldots, M-3, \end{cases}$$

as the case $i = 0$ corresponds to the pole $k = k_0$. The remaining $(M-2)(N+1)$ equations are derived along the inner edge of the ring $\rho = r_1$

$$\pi \mathrm{i} K r_1 \sum_{m=1}^{M} \frac{\left(\mathcal{D}\kappa_m^4 - \mu\right) k_i^2}{(k_i^2 - \kappa_m^2)(k_i^2 h - K^2 h + K)} \times \Big[k_i \mathrm{J}_{n+1}(k_i r_1) \left(a_{mn}^{(1)} \mathrm{H}_n^{(1)}(\kappa_m r_1) + a_{mn}^{(2)} \mathrm{H}_n^{(2)}(\kappa_m r_1) \right) - \kappa_m \mathrm{J}_n(k_i r_1) \left(a_{mn}^{(1)} \mathrm{H}_{n+1}^{(1)}(\kappa_m r_1) + a_{mn}^{(2)} \mathrm{H}_{n+1}^{(2)}(\kappa_m r_1) \right) \Big] = 0. \tag{39}$$

Thus, we have now derived $2(M-2)(N+1)$ relations (38–39) to determine the unknown amplitudes. The set of equations, like in the previous section, is completed by $4(N+1)$ edge conditions (28). The deflection can now be computed by (21).

The finite water-depth model can be used to solve the problem of shallow or infinitely deep water. Taking the limits $h \to 0$ and $h \to \infty$ we can derive the solutions for these situations including transition from the dispersion relation for water of finite depth to the dispersion relations for deep and shallow water, respectively.

8. Free-surface elevation and initiated wave pattern

We continue the analysis of the plate-water interaction and consider the open water regions, that consists of the main region $\mathcal{F}_0$ and the gap inside the ring $\mathcal{F}_1$. The elevation $\zeta(\rho, \varphi)$ of the free surface can be computed by (14), where the value of ζ^{inc} may be obtained from the incident wave potential expression (11) by use of the kinematic condition (2) and the value of ζ^{pm} from the following analysis of IDE in the water area.

The integro-differential equation has the form (37) for the FWD case. Therefore, we obtain the following expression for the free-surface elevation

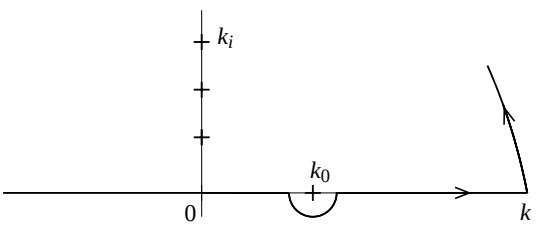

Figure 4. Closure of the contour of the integration in the upper half-plane.

$$\zeta(\rho,\varphi) = A\mathrm{e}^{\mathrm{i}k_0\rho\cos\varphi} - K\int\limits_{\mathcal{L}'}\sum_{m=1}^{M}\left(\mathcal{D}\kappa_m^4-\mu\right)\frac{\mathrm{J}_n(k\rho)}{(k^2-\kappa_m^2)} \times \sum_{i=0}^{M-3}\frac{k_i^2}{(k_i^2h-K^2h+K)(k-k_i)}\left[a_{mn}^{(1)}c_{mn}^{(1)}+a_{mn}^{(2)}c_{mn}^{(2)}\right]\mathrm{d}k. \tag{40}$$

We notice that in the open water region $\mathcal{F}_0$, where $\rho > r_0 > r_1$, $\mathrm{J}_n(k\rho)$ is split up into a half-sum of corresponding Hankel functions to close the contour of integration, and to do so at the gap area $\mathcal{F}_1$ the Bessel functions $\mathrm{J}_t(kr_1)$, $t=n, n+1$, are split up for $\rho < r_1 < r_0$. Finally, after using of the residue lemma at the poles $k=k_i$, we obtain for the free-surface elevation

$$\zeta(\rho,\varphi) = A\mathrm{e}^{\mathrm{i}k_0\rho\cos\varphi} - \pi\mathrm{i}\sum_{m=1}^{M}\left(\mathcal{D}\kappa_m^4-\mu\right) \times \sum_{i=0}^{M-3}\frac{k_i^2K}{(k_i^2h-K^2h+K)(k_i^2-\kappa_m^2)}\left[a_{mn}^{(1)}f_{mni}^{(1)}+a_{mn}^{(2)}f_{mni}^{(2)}\right], \tag{41}$$

where the functions $f_{mni}^{(q)}$ have the following forms in the open water $\mathcal{F}_0$ and in the gap $\mathcal{F}_1$

$$f_{mni}^{(q)} = \begin{cases} r_0\mathrm{H}_n^{(1)}(k_ir_0)\left[k\mathrm{J}_{n+1}(k_ir_0)\mathrm{H}_n^{(q)}(\kappa_mr_0)-\kappa_m\mathrm{J}_n(k_ir_0)\mathrm{H}_{n+1}^{(q)}(\kappa_mr_0)\right] & \text{in } \mathcal{F}_0, \\ r_1\mathrm{J}_n(k_i\rho)\left[k\mathrm{H}_{n+1}^{(1)}(k_ir_1)\mathrm{H}_n^{(q)}(\kappa_mr_1)-\kappa_m\mathrm{H}_n^{(1)}(k_ir_1)\mathrm{H}_{n+1}^{(q)}(\kappa_mr_1)\right] & \text{in } \mathcal{F}_1, \end{cases} \tag{42}$$

for $q=1,2$ and $i=0,\ldots,M-3$.

For infinitely deep water the procedure, in general, is the same, but with the pole $k=k_0$ of the water dispersion relation only. We derve the following equation for the free-surface elevation

$$\zeta(\rho,\varphi) = A\mathrm{e}^{\mathrm{i}k_0\rho\cos\varphi} - \pi\mathrm{i}\sum_{m=1}^{M}\left(\mathcal{D}\kappa_m^4-\mu\right)\frac{k_0^2}{(k_0^2-\kappa_m^2)}\left[a_{mn}^{(1)}f_{mn0}^{(1)}+a_{mn}^{(2)}f_{mn0}^{(2)}\right], \tag{43}$$

where the functions $f_{mn0}^{(q)}$, $q=1,2$, are defined by formula (42), for $i=0$, for the water regions $\mathcal{F}_0$ and $\mathcal{F}_1$.

The expressions (41) and (43) are for the total free-surface elevation for the FWD and IWD cases. We can subtract the incident field and use the second terms in the right-hand sides of these expressions, representing ζ^{pm}, to study the resulting wave pattern which is generated by the plate motion.

9. Numerical results

In this section numerical results are given for the problem for both the IWD and the FWD models. Results are presented for relevant and practically important cases. We show results for the plate deflection w, free-surface elevation ζ and initiated wave pattern elevation ζ^{pm}, all normalized by the wave amplitude A. Calculations are based on the varied flexural rigidity D, while the plate radii r_1 and r_0, Poisson ratio $\nu=0{\cdot}25$ and ratio $m/\rho_w=0{\cdot}25$ m are constant. The wave amplitude is $A=1$ m, water depth and incident wave length are varied, leading to different values of the wave number k_0 and, respectively, of the frequency ω. In all given figures the values of the inner and outer radii are the following: $r_1=100$ m and $r_0=500$ m.

The number of the roots of the plate dispersion relation that are taken into account for the FWD case is $M = 10$. The computation of the Bessel and Hankel functions of complex argument must be done accurately. Problems may appear when the argument is smaller than the order of the function and when the argument is too large or too small. Our algorithm was based on the Amos package [14], with some modifications to increase the accuracy, and computations were performed using the Fortran compiler. Scaled functions were used, which remove the exponential behavior in both the upper and lower half-planes. The definitions and description may be found in [15]. For zero argument we have used table values of Bessel and Hankel functions. We take $N = 30$ as the highest order of the modes of the Bessel functions, *i.e.*, we consider Bessel and Hankel functions of order 0 to 30. The choice of the truncation parameters M and N was also justified by computational testing such as to ensure sufficient accuracy. More details about the number of the roots can be found in [8] and about the order of the Bessel functions in [6].

The amplitude coefficients $a_{mn}^{(1)}$ and $a_{mn}^{(2)}$, as well as the corresponding Hankel functions, decay rapidly. With the increase of the radii and, correspondingly, of the arguments of the functions or the flexural rigidity, the decay becomes faster.

In all figures the left subplot is denoted as (a), and the right as (b); if there are four subplots, then lower left is denoted as (c) and lower right as (d). All figures are symmetric about the x-axis because incoming plane waves propagate in the x-direction and their crests are parallel to the y-axis.

In Figures 5–6 numerical results are shown for the plate deflection for both cases of water depth. The wave length in the second figure is two times larger than in the first, while the plate parameters are constant. The plate deflection for larger values of the rigidity is shown in Figure 7.

Numerical results for the elevation of the free surface in the ring gap are given in Figure 8 for different wave lengths. In Figure 9 we show results for the initiated wave pattern, *i.e.*, for the free-surface elevation ζ^{pm}, generated by the motion of the plate, and total free-surface elevation. The subplots for the open water region $\mathcal{F}_0$ are given for the surface of the fluid domain of the radius r_f, for water of finite depth. In Figures 10–11 we show a complete set of results for the unknowns being studied in the paper. Results are given for the plate deflection (a), free-surface elevation (b) in $\mathcal{F}_1$, initiated wave pattern (c) and the free-surface elevation (d) in $\mathcal{F}_0$ for the IWD and FWD cases, respectively.

The propagation of the wave through the plate area can be clearly seen, especially for small values of the plate rigidity. The wave propagates with a curved wave front, as is observed very well for these cases when the wave length is much smaller than the outer diameter of the ring. In a zone close to the plate edges the deflection can be quite different from that in the main zone.

The plate deflection and its hydroelastic response to the wave field are highly dependent on the ratio between outer radius r_0 and the wave length λ. With decreasing water depth the results for the plate deflection and free-surface elevation are changing gradually, upon which the water depth h itself has a growing influence on the results. For smaller values of the plate rigidity or stiffness the plate deflection increases, which is demonstrated in Figures 5–7. If the wave length is decreasing, then the value of the deflection grows. The deflection is larger numerically when the water depth increases. Also, we found that computational results for large values of depth, $h > 100$ m, are almost independent of water depth. For deep water the depth itself does not have a strong influence on the results, and for this situation it is sufficient to take $M = 10$ as well.

We found that for a rigidity $\mathcal{D} > 10^7$ m^4 the plate behaves as a rigid body with significant influence on the surface waves, whereas for $\mathcal{D} < 10^3$ m^4 the plate has hardly any influence on

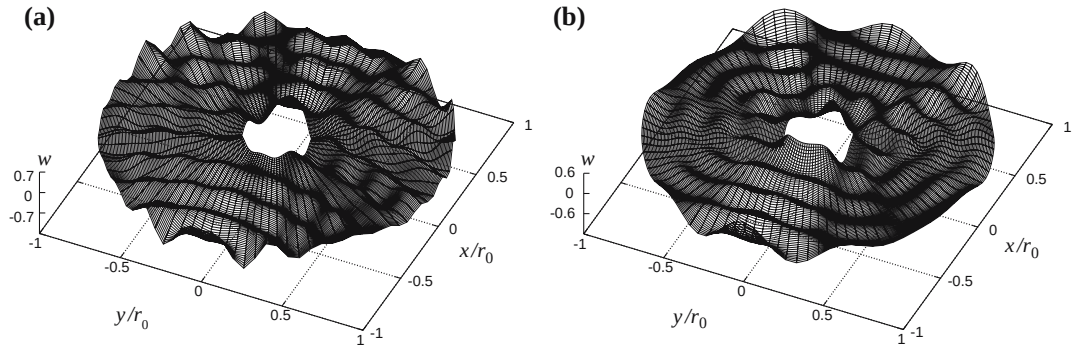

Figure 5. Deflection of the ring-shaped plate, for $\lambda = 50$ m, $\mathcal{D} = 10^5$ m^4: (a) infinite depth, (b) finite depth, $h = 20$ m.

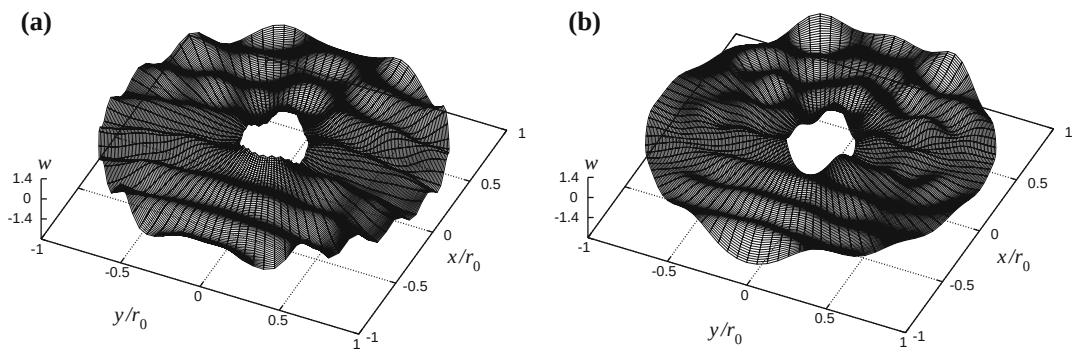

Figure 6. Plate deflection, as in Figure 5, for $\lambda = 100$ m.

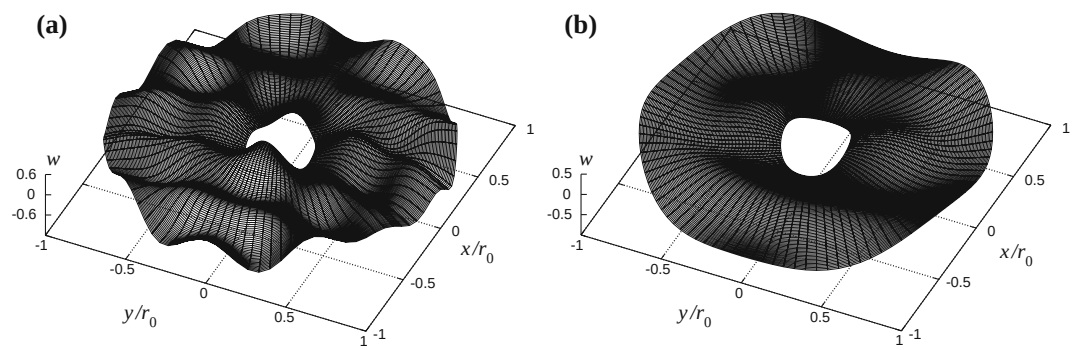

Figure 7. Plate deflection, for $\lambda = 100$ m, $h = 100$ m: (a) $\mathcal{D} = 10^6$ m^4, (b) $\mathcal{D} = 10^7$ m^4.

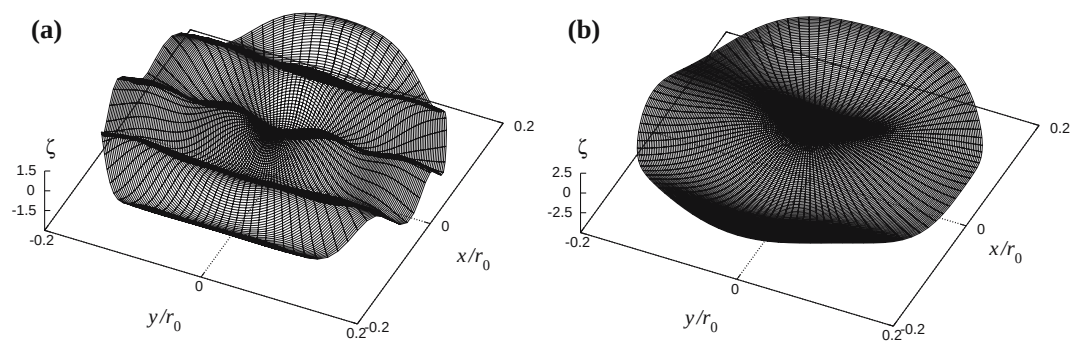

Figure 8. Free-surface elevation in the gap, for $h = 100$ m, $\mathcal{D} = 10^7$ m^4: (a) $\lambda = 50$ m, (b) $\lambda = 100$ m.

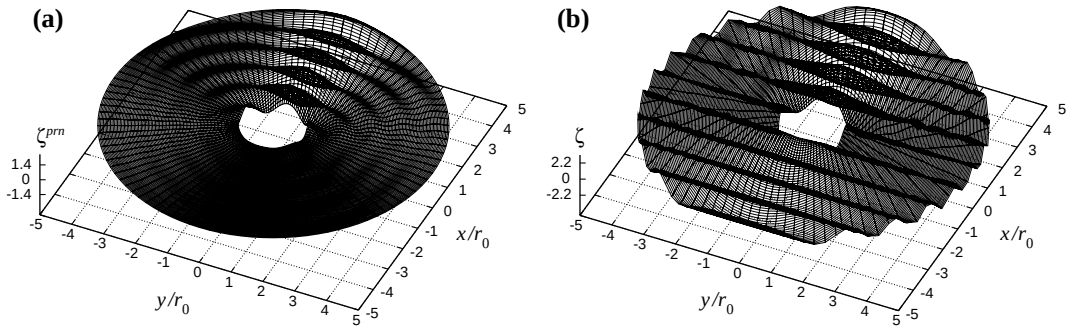

Figure 9. Initiated wave pattern (a) and free-surface elevation (b), for $\lambda = 500$ m, $h = 100$ m, $r_f = 2500$ m, $\mathcal{D} = 10^7$ m^4.

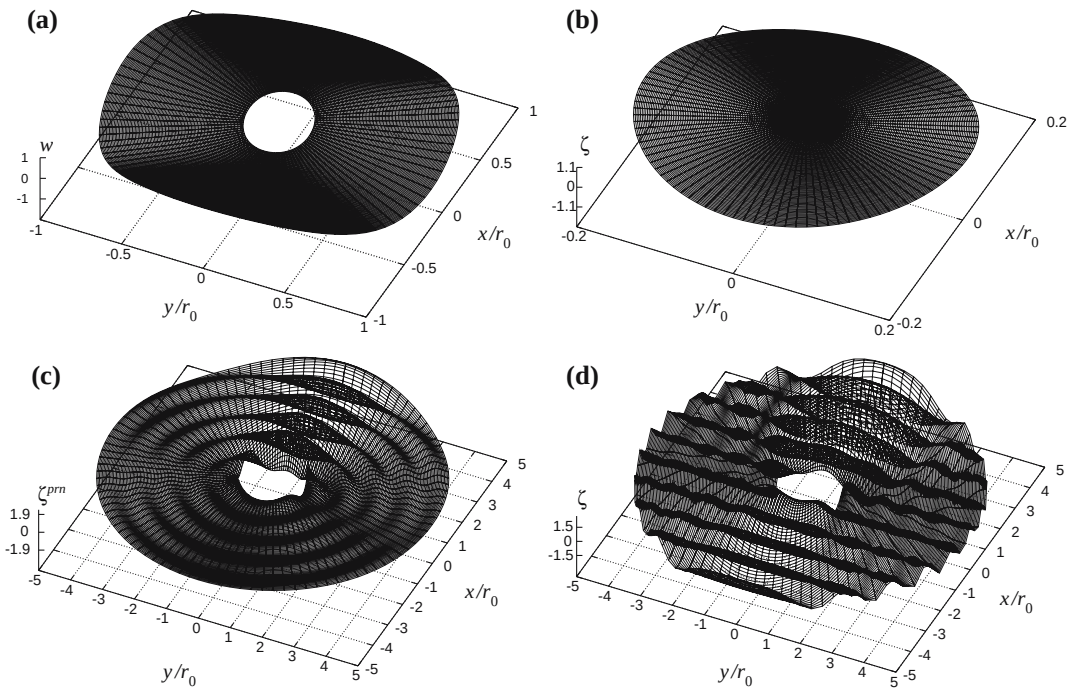

Figure 10. Deflection of the plate (a), free-surface elevation in $\mathcal{F}_1$ (b), initiated wave pattern (c) and free-surface elevation (d) in $\mathcal{F}_0$, for $\lambda = 500$ m, $h = 100$ m, $r_f = 2500$ m, $\mathcal{D} = 10^8$ m^4.

the incident surface waves. Realistic values of the rigidity for the VLFP can be of order of about 10^7 m^4; here many of the results shown for smaller values serve to demonstrate well the nature of plate-water interaction effects, while the rigidity for the ice can be of order of about 10^5 m^4.

The influence of the ring gap on the results is also shown. The propagated wave changes its behavior essentially after crossing the gap. The influence of the gap increases for smaller lengths of the wave.

The initiated wave pattern is highly dependent on water depth and the physical properties of the plate. For growing values of the plate flexural rigidity, stiffness or Poisson's ratio, the influence of the plate motion on the total elevation of the water surface is growing as well.

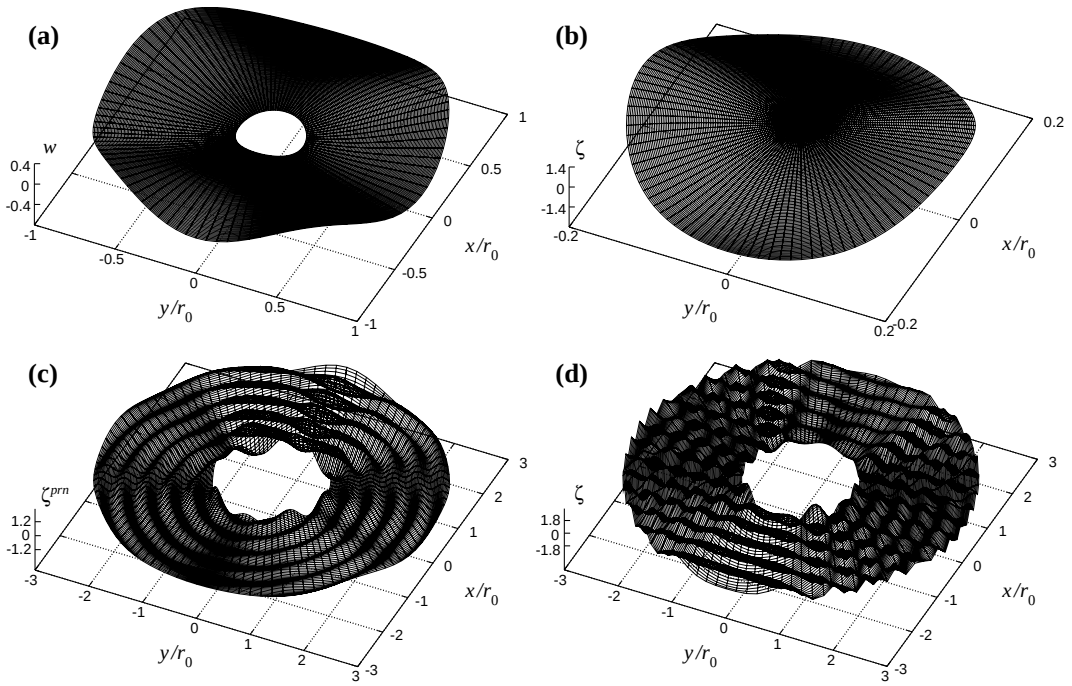

Figure 11. Deflection of the plate (a), free-surface elevation in $\mathcal{F}_1$ (b), initiated wave pattern (c) and free-surface elevation (d) in $\mathcal{F}_0$, for $\lambda = 200$ m, $r_f = 1500$ m, $\mathcal{D} = 10^8$ m^4.

10. Conclusions

The problem of the interaction between the floating thin elastic plate of a ring-shaped planform and incident surface water waves has been solved. An analytic and numerical study of the hydroelastic behavior of the plate has been presented. The integro-differential equation of the problem was derived and an algorithm of its numerical solution proposed. For the case of finite water depth the system of equations for the expansion coefficients has been obtained analytically. For infinitely deep water the problem has been solved partly.

The vertical displacements in the plate and water regions, the plate deflection and free-surface elevation, respectively, have been studied and obtained. The influence of the plate motion on the solution in the water regions was analyzed by the derivation of the initiated wave pattern. Also, the influence of the ring gap was analyzed and demonstrated. For realistic values of the plate mass and rigidity, the plate behavior does not differ much from that of a circular plate, except for the area behind the ring gap. In the inner free surface area $\mathcal{F}_1$ the resonant situation, that is, large free-surface elevation, is possible for some values of the wave length, see Figure 8, as was shown by Hermans [9] for the channel between two plates. This phenomenon is also demonstrated by Molin in his study of sloshing modes in a moonpool [16].

The solution for water of finite depth can be used for problems with shallow or very deep (infinite) water. The floating platform should be located in offshore zones of the ocean or sea. The water depth is rather small in such zones, but as wave lengths can be both short and long, it is more natural to use the finite-water-depth model to study the hydroelastic response of the plate to water waves.

The presented approach, particularly the analysis of the IDE and Green's function, is valid for any rotational symmetric configuration of the plate. The solution presented above is a

new application of the integro-differential formulation. This formulation allows us to solve many problems of interaction between water waves and floating bodies. The main goal of the method is the derivation of an integro-differential equation along the plate contour, followed by its analysis and solution. One of the advantages of our approach is that we may find both vertical displacements, the plate deflection in $\mathcal{P}$ and the free-surface elevation in $\mathcal{F}$, using a common set of equations.

The presented approach is valid when the plate draft and thickness are assumed to be zero. So, the next task to study is the interaction of incoming water waves and plates of finite thickness.

A possible application of the method is to use it for the hydroelastic analysis of the VLFP. The planform of the VLFP depends on the water depth, currents of the sea or ocean, where a floating airport could be located, distance from the coast, etc. In some cases it can make sense to construct the VLFP of an arbitrary horizontal shape. One can also use the presented approach to study the motion of large ice fields in water waves, using the physical properties of the ice instead of those of the elastic plate. Most results are presented for the large plate, $2r_0 > \lambda$, but the approach is also valid for small-sized floating plates $2r_0 < \lambda$, which may be used for different purposes in the sea.

References

1. E. Watanabe, T. Utsunomiya and C.M. Wang, Hydroelastic analysis of pontoon-type VLFS: a literature survey. *Eng. Struct.* 26 (2004) 245–256.
2. G. Zilman and T. Miloh, Hydroelastic buoyant circular plate in shallow water: a closed form solution. *Appl. Ocean Res.* 22 (2000) 191–198.
3. T. Tsubogo, The motion of an elastic disk on shallow water in waves. In: J.S. Chung, M. Sayeed, H. Saeki and T. Setoguchi (eds.), *Proceedings of 11th International Offshore and Polar Engineering Conference*. Vol. 1. Stavanger, Norway (2001) pp. 229–233.
4. E. Watanabe, T. Utsunomiya, C.M. Wang and Y. Xiang, Hydroelastic analysis of pontoon-type circular VLFS. In: J.S. Chung and S. Prinsenberg (eds.), *Proceedings of 13th International Offshore and Polar Engineering Conference*. Vol. 1. Honolulu, USA (2003) pp. 93–99.
5. M.A. Peter, M.H. Meylan and H. Chung, Wave scattering by a circular plate in water of finite depth: a closed form solution. In: J.S. Chung and S. Prinsenberg (eds.), *Proceedings of 13th International Offshore and Polar Engineering Conference*. Vol. 1. Honolulu, USA (2003) pp. 180–185.
6. A.I. Andrianov and A.J. Hermans, Hydroelasticity of a circular plate on water of finite or infinite depth. *J. Fluids Struct.* 20 (2005).
7. A.J. Hermans, The ray method for the deflection of a floating flexible platform in short waves. *J. Fluids Struct.* 17 (2003) 593–602.
8. A.I. Andrianov and A.J. Hermans, The influence of water depth on the hydroelastic response of a very large floating platform. *Marine Struct.* 16 (2003) 355–371.
9. A.J. Hermans, Interaction of free-surface waves with floating flexible strips. *J. Engng. Math.* 49 (2004) 133–147.
10. S.P. Timoshenko, D.H. Young and W. Weaver, *Vibration Problems in Engineering*. New York: John Wiley & Sons (1974) 521 pp.
11. J.V. Wehausen and E.V. Laitone, Surface waves. In: W. Flügge (ed.), *Encyclopedia of Physics*. Vol. 9. Berlin: Springer-Verlag (1960) pp. 446–814. (*Also at http://www.coe.berkeley.edu/SurfaceWaves*).
12. C.J. Tranter, *Bessel Functions with Some Physical Applications*. London: The English Universities Press (1968) 148 pp.
13. G.A. Korn and T.M. Korn, *Mathematical Handbook for Scientists and Engineers: Definitions, Theorems and Formulas for Reference and Review*. New York: McGraw-Hill (1968), 831 pp.
14. D.E. Amos, A portable package for Bessel functions of a complex argument and nonnegative order. *ACM Trans. Math. Software* 12 (1986) 265–273.
15. M. Abramowitz and I.A. Stegun, *Handbook of Mathematical Functions with Formulas, Graphs, and Mathematical Tables*. Washington: U.S. Government Printing Office (1964) 1046 pp.
16. B. Molin, On the piston and sloshing modes in moonpools. *J. Fluid Mech.* 430 (2001) 27–50.